Isentropic Decompression of Fluids From Crustal and Mantle Pressures

SUSAN WERNER KIEFFER[1] AND JOAN MARIE DELANY

Department of Earth and Space Sciences, University of California, Los Angeles, California 90024

Possible thermodynamic histories of H_2O and CO_2 decompressing isentropically from crustal and upper mantle pressures are examined using graphs of entropy versus density with contours of constant pressure and mass fraction. These graphs are particularly useful for problems in dynamic processes because, in addition to providing thermodynamic information about entropy, density, pressure, phase, and—if more than one phase is present—mass fraction vapor, the graphs allow visualization of the sound speed, the parameter which controls the rate of propagation of disturbances in many fluid dynamics and geophysical problems. The sound speed is represented by the vertical gradient of the isobars on the entropy-density graphs and is thus easily envisioned across phase changes or as a function of pressure, mass fraction vapor, or density, as the 'topography' represented by the isobaric contours. This representation is especially useful for illustrating the low sound speeds of two-phase liquid-gas systems, e.g., the speed of a few meters per second characteristic of water-steam mixtures at 1-bar pressure as contrasted to 1500 m s^{-1} in liquid water or 450 m s^{-1} in steam. Two simple inequalities are derived from conservation of energy, mass, and momentum to clarify conditions under which flow processes in single-component, single-phase systems are 'approximately isentropic.' Application of these inequalities to specific problems of gas dynamics, ascent of magma and shock decompression of gases, liquids, and solids suggests that under many realistic conditions, rapid magma emplacement and shock decompression of gases and liquids may be considered to be approximately isentropic processes. However, shock decompression of solids is probably not an isentropic process because viscous dissipation could contribute significantly to entropy production and to volume changes not accounted for in an isentropic equation of state. Entropy-density graphs of H_2O along representative crustal geotherms show that isentropic ascent of H_2O from crustal depths causes partial vaporization of a liquid phase as pressures decrease toward the surface pressure of 1 bar, whereas isentropic ascent from greater depths (pressures greater than 20–50 kbar, depending on the geotherm chosen) causes partial condensation of a vapor phase near the surface. A comparison of the thermodynamic history of H_2O and CO_2 originating at depths characteristic of kimberlite or carbonatite source regions shows that H_2O goes through a condensation phase change near the surface (supercritical fluid → vapor → vapor + liquid) but CO_2 expands entirely into the vapor-alone field. Because the condensation phase change in the H_2O system might significantly alter fluid flow properties, H_2O and CO_2 cannot be considered to behave in a qualitatively similar manner in the dynamics of eruption of kimberlite or carbonatite. The entropy-density graphs are also used to examine the isentropic release of H_2O from shock Hugoniot states, under the commonly used assumption that thermodynamic equilibrium is maintained. Upon release from pressures below 275 kbar, partial vaporization of a liquid phase occurs; upon release from higher pressures, partial condensation of a vapor phase occurs.

1. INTRODUCTION

The behavior of materials under rapid decompression, either from crustal pressures, as in the case of volcanism, or from even higher pressures, as in the case of meteorite impact, is strongly determined by the sound speed of the decompressing medium (for example, see *McGetchin and Ullrich* [1973], *Sanford et al.* [1975], *Kieffer* [1975, 1977*a*] for discussions of the effect of sound speed during volcanic or geyser eruptions; see *Zeldovich and Razier* [1966, chapter 1], for a discussion of decompression from shock states). In many cases the decompressing materials are multiphase, single- or multiple-component mixtures, such as water-steam or magma-gas mixtures. The sound speeds of multiphase mixtures are generally such complex functions of many variables (the proportions of phases present, pressure, temperature, bubble size, latent heat, and degree of equilibrium [*Kieffer*, 1977*b*]) that simple representation of the sound speed as a function of these variables is difficult. This paper introduces a simple graphical representation of sound speeds in multiphase systems and demonstrates the thermodynamic and fluid dynamic conclusions which can be obtained from the representation.

The speed of sound is an important fluid dynamics parameter because it is the velocity at which small disturbances are propagated in a material. Thus, for example, if we ask about the rate at which a disturbance such as a vent opening or pressure release is propagated into a magma chamber, the sound speed of the magma must be known before the answer can be determined. The 'dynamic' variable, the sound speed, depends on the 'static' state variables (pressure P, density ρ, and entropy S) through the identity

$$c^2 = \left(\frac{\partial P}{\partial \rho}\right)_S \tag{1}$$

This can be demonstrated as follows (after *Zeldovich and Razier* [1966] or many fluid dynamics texts):

Consider the density and pressure to be written as their undisturbed values ρ_0 and P_0, respectively, plus small changes $\Delta\rho$ and ΔP, accompanying the fluid motion. For a uniform fluid and, for simplicity, for a one-dimensional case, the Eulerian equation of continuity gives

$$\frac{\partial \Delta\rho}{\partial t} = -\rho_0 \frac{\partial u}{\partial x} \tag{2}$$

and the equation of motion is

$$\rho_0 \frac{\partial u}{\partial t} = -\frac{\partial P}{\partial x} = -\left(\frac{\partial P}{\partial \rho}\right)_S \frac{\partial \Delta\rho}{\partial x} \tag{3}$$

where t is time, x is the spatial coordinate, u is the particle velocity (assumed to be small), and S is entropy. In all formu-

[1] Now at U.S. Geological Survey, Flagstaff, Arizona 86001.

Paper number 8B1064.
0148-0227/79/008B-1064$01.00

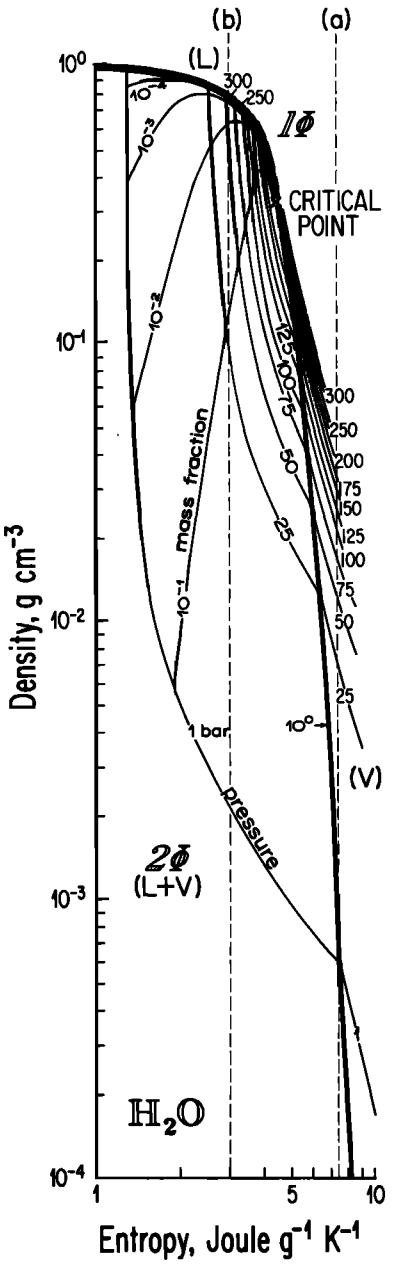

Fig. 1. Entropy-density relations for H_2O. Entropy is relative to a triple-point entropy, S (triple point) = 0. Data are from *Keenan et al.*'s [1969] steam tables. The single-phase field is shown as 1ϕ and the two-phase (liquid + vapor) field as 2ϕ. Contours of constant pressure (isobars) are shown in 25-bar increments. In the two-phase field, contours of constant mass fraction vapor (isopleths) are shown. Dashed lines (*a*) and (*b*) are discussed in the text; (*a*) intersects the two-phase region at 1-bar pressure.

lations it is assumed that the particle motions in the disturbance are isentropic, so that a small change in pressure is related to a small change in density by $\Delta P = (\partial P/\partial \rho)_S \Delta \rho$. Denote $(\partial P/\partial \rho)_S$ as c^2 without, for the moment, any connotation of sound speed. A simple wave equation can be obtained from (2) and (3) by differentiating (2) with respect to time, and (3) with respect to x and eliminating $\partial^2 u/\partial t\, \partial x$. The resulting equation has the form of a classical wave equation:

$$\frac{\partial^2 \Delta\rho}{\partial t^2} = c^2 \frac{\partial^2 \Delta\rho}{\partial x^2} \tag{4}$$

The equation (and similar equations for ΔP and u) have two families of solutions:

$$\Delta\rho = \Delta\rho(x - ct) \qquad \Delta P = \Delta P(x - ct) \qquad u = u(x - ct) \tag{5a}$$

$$\Delta\rho = \Delta\rho(x + ct) \qquad \Delta P = \Delta P(x + ct) \qquad u = u(x + ct) \tag{5b}$$

where c is the positive root, $c = +(\partial P/\partial \rho)_S^{1/2}$. These solutions describe disturbances which propagate in the positive and negative x directions with the velocity c, e.g., in the first family of solutions above, $\Delta\rho$, ΔP, or u are constant if $x = ct$ + const, and the disturbance $\Delta\rho$ or ΔP therefore propagates in the $+x$ direction. Therefore c is the speed at which disturbances are propagated through materials.

This brief review is a reminder that, although the derivative $(\partial P/\partial \rho)_S$ is normally thought of in terms of the compressibility, $K = \rho(\partial P/\partial \rho)_S$, a static parameter, it is important in the form $c^2 = (\partial P/\partial \rho)_S$ in dynamic problems as well. In cases where the sound speed has been determined from pressure-density data at constant entropy and compared with the sound speed determined from dynamic ultrasonic data, the agreement between the static and dynamic methods is good to within about 10% (the comparison shown by *Kieffer* [1977*b*, Figure 2] is typical). Differences may be due to experimental uncertainties, dissipation in a dynamic experiment, or dispersion (frequency dependence).

Isentropic processes are not only of geologic interest in the propagation of small-amplitude disturbances as discussed above, but also in a number of problems involving large pressure, density, or temperature disturbances. In these problems, processes which can be demonstrated to be adiabatic ($dQ = 0$, where dQ is the heat transferred) are frequently assumed to be isentropic ($dS = 0$, where dS is the entropy change). Two examples of processes assumed to be adiabatic and isentropic are ascent of magma [*Rumble*, 1976] and release from shock compression during meteorite impacts and laboratory shock experiments [*Rice and Walsh*, 1957; *McQueen and Marsh*, 1960; *Ahrens and Rosenberg*, 1968]. Although adiabatic processes, being irreversible, are not necessarily isentropic (see discussion below), the assumption of constant entropy so greatly simplifies the mathematical and thermodynamic treatment of many problems, particularly those of geologic systems for which material properties are complex, that it is useful to apply the isentropic assumption whenever reasonably justified. Thus in section 2 of this paper we consider a criterion according to which processes may be considered 'approximately isentropic.'

We describe in section 3 entropy-density graphs which we have found offer a simple visual representation of a number of thermodynamic variables involved in isentropic processes. In section 4 we demonstrate how the graphs can be used to examine the behavior of volatiles (1) ascending in volcanic systems originating at different depths within the earth, and (2) decompressing from a shock Hugoniot state. Entropy-density graphs for the two systems considered, H_2O and CO_2, are presented in Figures 1 and 2, respectively.

2. Isentropic Processes

We propose below criteria which might be used to check if single-component, single-phase flows are 'approximately isentropic.' In the following discussion it is assumed that the usual results of thermodynamics can be applied to material motions. This can generally be done if the instantaneous local thermodynamic state is considered and if the rates of change of the parameters describing the local state are not

too large. In particular, it is assumed that the characteristic times of the problem (t_0) are larger than relaxation times (τ) for material changes (such as phase changes, nucleation and growth processes, etc.), so that flows are 'slow' in terms of departure from thermodynamic equilibrium. (The word slow takes on a wide range of values, depending on whether the relaxation times are those associated with molecular translations, rotations, vibrations, or dissociations in gas flow ($\tau = 10^{-10}$–10^{-5} s) or those of nucleation and growth of metamorphic minerals in viscous solids (τ perhaps as large as 10^{14} s)!) It is also assumed that the substances considered are fluidlike in that they cannot support shear stresses and that they are described by linear stress and heat conduction relations.

Similar criteria for isentropic flow have been given by *Batchelor* [1967, pp. 164–171] and *Thompson* [1972, chapter 3]. The criteria follow from consideration of the total material derivative of a generalized equation-of-state of the form $P = P(\rho, S)$:

$$\frac{DP}{Dt} = \left(\frac{\partial P}{\partial \rho}\right)_S \frac{D\rho}{Dt} + \left(\frac{\partial P}{\partial S}\right)_\rho \frac{DS}{Dt} \tag{6a}$$

or

$$\frac{DP}{Dt} = c^2 \frac{D\rho}{Dt} + \left(\frac{\partial P}{\partial S}\right)_\rho \frac{DS}{Dt} \tag{6b}$$

In these expressions, D/Dt is the total derivative, P is pressure, ρ is density, S is entropy, c is the adiabatic sound speed, and t is time. For an isentropic process, S is constant and therefore the equation-of-state is a function of density only, $P = P(\rho)$. This would be true in the equations above if

$$\left| c^2 \frac{D\rho}{Dt} \right| \gg \left| \left(\frac{\partial P}{\partial S}\right)_\rho \frac{DS}{Dt} \right| \tag{7}$$

The partial derivatives on the right-hand side can be expressed in terms of the fluid flow parameters through use of the continuity, momentum, and energy equations. As there are subtle assumptions about the relative magnitudes of forces, circumstances of the particular flow under consideration, and properties of the fluid in the following section, the reader is referred to *Thompson* [1972, pp. 138–144] for details. For example, the equations take account of the gravitational field, but it is not important if $l_0 \ll c_0^2/g$, where l_0 is a characteristic length, c_0 is the sound speed, and g is the acceleration of gravity. It is assumed negligible in the following discussion. The resulting approximation for flow to be considered approximately isentropic is

$$|\nabla \cdot \mathbf{u}| \gg \left| \frac{1}{C_P} \left(\frac{\partial v}{\partial T}\right)_P [\Gamma + k \nabla^2 T] \right| \tag{8}$$

where $\mathbf{u}$ is the flow velocity, C_P is the specific heat, v is the volume, T is the temperature, Γ is the dissipation factor (which represents the part of the work going into deformation), k is the thermal conductivity, $\nabla \cdot \mathbf{u}$ is the divergence of the velocity ($\partial u/\partial x + \partial u/\partial y + \partial u/\partial z$ in Cartesian coordinates), and $\nabla^2 T$ is the Laplacian of the temperature ($\partial^2 T/\partial x^2 + \partial^2 T/\partial y^2 + \partial^2 T/\partial z^2$ in Cartesian coordinates). The physical interpretation of this equation is that the overall rate of volume change (on the left-hand side of the equation) must be large compared to the rate of volume change due to viscous heating (first term on the right) and thermal conduction (second term on the right) for an isentropic process. The equation is most easily considered for general situations by forming nondimensional variables as follows:

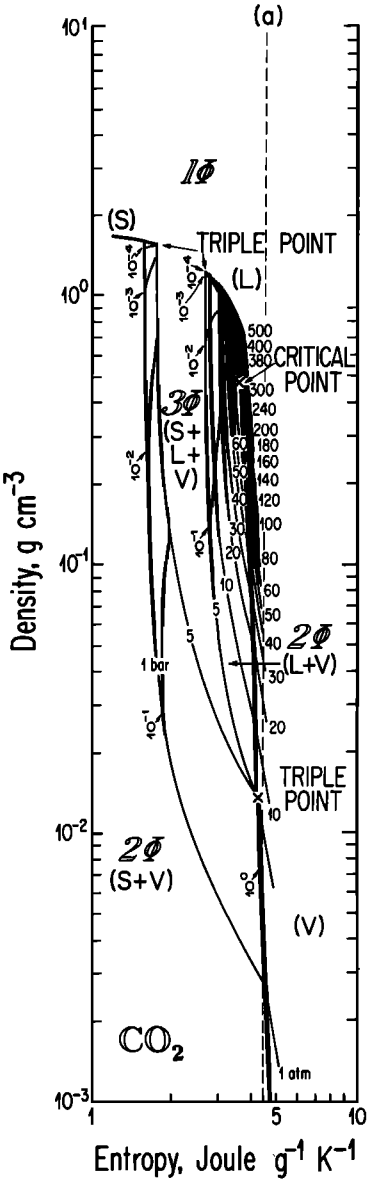

Fig. 2. Entropy-density relations for CO_2. Entropy is relative to $S(0\,\mathrm{K}) = 0$. Data are from *Newitt et al.* [1956]. The single-phase field is shown as 1ϕ; the two-phase regions (solid + vapor) and (liquid + vapor) as 2ϕ; and the three-phase region bounded by the triple-point wedge as 3ϕ. Note the small area of the (solid + vapor) field which lies below the lower triple point, at higher entropies and lower densities than the (liquid + vapor) field. Contours of constant pressure (isobars) are shown in 10-bar increments at pressures greater than 10 bars. In the two-phase field, contours of constant mass fraction vapor (isopleths) are shown. Dashed line (*a*) intersects the two-phase region at 1-bar pressure.

$$\mathbf{U} = \mathbf{u}/u_0 \qquad \tilde{\Gamma} = l_0^2 \Gamma/\mu u_0^2 \qquad \tilde{T} = T/T_0$$

$$Re = \rho_0 u_0 l_0/\mu = u_0 l_0/\nu \qquad Pr = \mu C_P/k = \nu/\kappa$$

where the length l_0 chosen is a characteristic length over which a characteristic velocity change u_0, and a characteristic temperature change T_0, are obtained (in a time t_0), i.e., spatial differentiation of a quantity is assumed to change its magnitude by l_0^{-1}. We assume a Newtonian fluid and denote by μ the ordinary shear viscosity and ν the kinematic viscosity; ρ_0 is the reference density and κ is the thermal diffusivity. Re is the classical Reynolds number and Pr is the Prandtl number. The

nondimensional form of the condition that a flow process be approximately isentropic is then

$$|\nabla\cdot\mathbf{U}| \gg \left|\frac{1}{Re}\frac{T}{v_0}\left(\frac{\partial v}{\partial T}\right)_P\left(\frac{u_0^2}{C_PT_0}\tilde{\Gamma}+\frac{1}{Pr}\nabla^2\tilde{T}\right)\right| \quad (9)$$

(Here v_0 is the specific volume, $1/\rho_0$.) In general, $|\nabla\cdot\mathbf{U}| \ll (u/u_0) \div (x/l_0)$ and, specifically, $\nabla\cdot\mathbf{U} = 0$ for incompressible flow. However, if the flow is compressible, then $\nabla\cdot\mathbf{U} \sim 1$. We assume from here on that we are dealing with fluid flow situations in which compressibility is important. If the dimensionless variables have been properly chosen, then $\nabla^2\tilde{T}$ and $\tilde{\Gamma}$ are approximately unity and the inequality becomes

$$1 \gg \left|\frac{1}{Re}\frac{T}{v_0}\left(\frac{\partial v}{\partial T}\right)_P\left(\frac{u_0^2}{C_PT_0}+\frac{1}{Pr}\right)\right| \quad (10a)$$

Therefore only four dimensionless parameters determine whether or not the flow is approximately isentropic: (1) the ratio of inertial to viscous forces given by the Reynolds number; (2) the dimensionless volume change given by $T/v_0\cdot(\partial v/\partial T)_P = T\alpha$, where α is the thermal expansion coefficient; (3) the ratio of kinetic to internal energy given by u_0^2/C_PT; and (4) the ratio of viscous to thermal diffusivity given by the Prandtl number. If it is assumed that the two terms on the right-hand side do not cancel at all points in the flow field, (10*a*) reduces to the two subsidiary conditions

$$\left|\frac{1}{Re}T\alpha\frac{u_0^2}{C_PT}\right| \ll 1 \quad (10b)$$

(the viscous inequality) and

$$\left|\frac{1}{Re}T\alpha\frac{1}{Pr}\right| \ll 1 \quad (10c)$$

(the thermal inequality)

Special Cases

Gases. In general, for gases, $T\alpha \sim 1$, so (10*b*) and (10*c*) reduce further to

$$\left|\frac{1}{Re}\frac{u_0^2}{C_PT_0}\right| \ll 1 \quad (11a)$$

and

$$\left|\frac{1}{Re}\frac{1}{Pr}\right| \ll 1 \quad (11b)$$

Equation (11*a*) is commonly written in terms of the Eckert number E (which, for example, for a perfect gas is $E = (\gamma - 1)M^2$, where γ is the adiabatic exponent and M is the Mach number). Equation (11*a*) then becomes $E/Re \ll 1$. For many gases, $Re \approx M_0l_0/\Lambda_0$, where M_0 is the Mach number, u_0/c, and Λ_0 is the molecular mean free path. The ratio l_0/Λ_0 is usually large in physical situations where a continuum model for material properties is applied, so even for fairly small Mach number the Reynolds number of gas flow is large. Since u_0^2/C_PT_0 is of order 1 only for supersonic flows (which are also high Reynolds number), it can be seen that (11*a*) is satisfied for most gas flows. Similarly, since the Prandtl number for gases is in the range 2/3–1 [*Thompson*, 1972, p. 110], the inequality (11*b*) is also satisfied for most gas flows. Thus to a good approximation, flow problems typically considered in classical compressible gas dynamics are justifiably considered to be isentropic.

Liquids and solids. At temperatures below 3000 K, $T\alpha$ for liquids and solids may be expected to be of order 0.1 or less, so (10*a*) and (10*b*) become slightly less restrictive than for gases:

$$\left|\frac{1}{Re}\frac{u_0^2}{C_PT_0}\right| \ll 10 \quad (12a)$$

and

$$\left|\frac{1}{Re}\frac{1}{Pr}\right| \ll 10 \quad (12b)$$

Generalization beyond these equations is not warranted because processes of geologic interest can involve Reynolds numbers ranging from 10^{-17} to 10^{6} (at least) and Prandtl numbers ranging from 1 to 10^{20}. The samples of fluid flow considered in this paper are (1) ascent of fluids or magma in volcanic eruptions and (2) decompression of fluids from the shock state.

Ascent of magma: Viscosities of magmas vary from 10^2 to 10^4 P for basaltic or andesitic magmas to 10^6–10^9 P for granitic magmas. Basaltic magmas frequently exhibit high Reynolds number flow when they are observed on the surface, e.g., in Hawaiian lava rivers where u_0 can be 10^3 cm s^{-1} and l_0 about 10^3 cm, the Reynolds number will be greater than unity for viscosities less than 10^6, i.e., for most basaltic magmas. *Shaw* [1965, p. 138] has postulated that emplacement of granitic magmas may also occur at Reynolds numbers appreciably greater than unity, as high as 10^3. Therefore most magma emplacement and flow conditions (to the extent that they can be idealized as single-component, single-phase systems) may be approximately isentropic, the most notable exception being emplacement of granitic magmas at low Reynolds numbers.

The ascent of volatiles with or through a magma must be considered separately. If the volatiles comprise a small volume fraction of the magma, and if they are dispersed in small vesicles of a separate liquid or gas phase, heat transfer between the volatile phase and the silicate phase might make the ascent of the volatile phase more nearly isothermal than adiabatic. Even though the total entropy of the system might be constant, the entropy of the individual phases might vary. Thus when the volatile fraction is small, the real ascent behavior may lie between isothermal and adiabatic.

For large volatile contents, as in eruptions of kimberlites and carbonatites, or perhaps as in phreatic explosions, a dispersed solid and/or liquid phase may be thermally decoupled from the gas phase. In this case, the dispersed phase may appreciably alter the effective viscosity but not otherwise influence the thermal behavior of the flow. It is to such cases that the discussion of volatile decompression in section 4 of this paper applies.

Decompression following shock waves: It is commonly assumed that decompression of gases, liquids, and solids following shock comparison is isentropic [*Bradley*, 1962, chapter 2; *McQueen and Marsh*, 1960]. The inequalities (11*a*) and (11*b*) are generally satisfied for expanding gases because the Prandtl number is of the order unity and the Reynolds number is usually very high. Inequalities (12*a*) and (12*b*) should be satisfied for low-viscosity liquids ($\mu < 10^4$ P). Therefore the isentropic thermodynamic paths discussed in the next section of this paper for H_2O and CO_2 liquids and gases may be expected to approximate the real thermodynamic history obtained in shock release paths, if local thermodynamic equilibrium is obtained.

It is not clear that the decompression of solids by rarefaction waves is approximately isentropic. Thermal conduction effects

are not important: notice that the thermal inequality (12*b*) reduces to become independent of the viscosity:

$$\left|\frac{1}{Re}\frac{1}{Pr}\right| = \frac{\kappa}{u_0 l_0} \ll 10 \tag{13}$$

For $\kappa \sim 10^{-3}$ cm^2 s^{-1} and characteristic rarefaction velocities of 1 km s^{-1}, this inequality holds for all characteristic distances l_0 greater than 10^{-9} cm, and hence entropy production and volume changes due to thermal conduction are negligible (as is commonly recognized in the assumption of the adiabatic nature of shock flow).

It is not equally obvious that the viscous inequality (12*a*) can be satisfied. A major problem in consideration of this is our lack of knowledge of effective viscosity of solids at the high strain rates characteristic of shock processes, but a few limits can be placed on viscosities which would result in satisfaction of the inequality (12*a*). For $u_0 \sim 1$ km s^{-1} and $u_0^2/C_P T_0 \sim 1$, (12*a*) simply requires that $\nu \ll 10^6 l_0$ (l_0 in centimeters). If l_0 is as large as 1 cm (which it probably is not), then $\nu < 10^6$ P, i.e., the viscosity must be less than that of, say, andesitic magma. Since l_0 is probably much smaller than 1 cm, a correspondingly lower viscosity is required. It is not apparent that the compressed solid undergoing decompression can attain such low viscosities by any known mechanism (e.g., formation of thetomorphic glass, glass lamellae, dislocation motion). On the other hand, it has not been demonstrated here that deviations from isentropeticity would cause measurable changes in shock equation-of-state parameters, such as free surface particle velocities or release volumes. In summary, we recommend that the assumption of isentropic flow in decompressing solids be critically examined to determine if viscous dissipation is contributing significantly to entropy production and to volume changes not accounted for in an isentropic equation of state.

We reemphasize here that this discussion has been restricted to single-component, single-phase systems and that generalization of (6)–(13) is required for application to multicomponent or multiphase systems.

3. Description of the Graphs

Consider first the entropy-density graphs for H_2O shown in Figure 1. The saturation curve is shown as a heavy line separating the two-phase region in the lower left (labeled as 2ϕ) from the liquid-alone and the vapor-alone regions on the right and top (labeled as 1ϕ). At entropies less than the critical point entropy, the single phase is liquid and the heavy curve represents the boundary between liquid and (liquid + vapor) regions. At entropies greater than the critical point entropy, the single phase is vapor and the heavy curve is the boundary between vapor and (vapor + liquid) regions.

On the entropy-density graph of CO_2 (Figure 2) the saturation curve is also shown as a heavy line separating the two-phase and one-phase regions. At entropies less than the critical point entropy, liquid is in equilibrium with (liquid + vapor) across the saturation curve; at entropies greater than the critical point entropy, vapor is in equilibrium with (vapor + liquid) across the curve. CO_2 differs from H_2O in that it has a triple point at pressures of geological interest: at 5.1 bars, −56.6°C. In entropy-density space the triple point appears as a wedge-shaped region cutting up toward the left in Figure 2; it is open at the top end because of the entropy and density discontinuities between the liquid and solid phases at the triple point. At the far upper left the solid-vapor saturation curve of 'dry ice' is shown. The solid-liquid curve cannot be shown because only a portion of the melting curve of CO_2 has been measured [*Bridgman*, 1914] and because entropies and volumes for the solid and liquid phases along the melting curve have not, to our knowledge, been measured.

It is the addition of contours of the intensive thermodynamic variables, pressure and mass fraction, onto these graphs which makes them useful for solution of problems relating to flow processes. The lines which cut across both figures, generally from upper left to lower right, are isobars. The lines which cut across, generally toward the upper right but with strong curvatures toward the saturation curve, are isopleths of mass fraction vapor. Isopleths cannot be plotted through the wedge-shaped region bounded by the triple point for CO_2 because of the lack of thermodynamic data on the liquid-solid equilibrium curve.

The graphs are useful for representation of isentropic processes and associated changes of state and thermodynamic variables. Isentropic processes are represented by vertical lines on these graphs and isentropic decompression by paths from top to bottom. Phase changes and density changes with pressure increases or decreases during isentropic processes are easily seen. At any given pressure (read from the isobars) it is possible to read the total entropy, density, and, in the two-phase region, mass fraction of the phases. Furthermore, the sound speed which by definition is the directional derivative along vertical lines of constant entropy, $c = (\partial P/\partial \rho)_S^{1/2}$, is simply proportional to the vertical gradient of the isobaric contours. These graphs are constructed on a logarithmic scale because the great change of density possible for the vapor phase requires a logarithmic axis and the definition of sound speed requires that both axes then be logarithmic in order to preserve a direct proportionality:

$$2 \log c = \log \left(\frac{\partial P}{\partial \rho}\right)_S \tag{14}$$

For isobars, $\partial P = \text{const}$. Therefore if the spacing ($\partial \rho$) between isobars on an isentrope is large, c is small, and vice-versa.

By viewing these graphs as 'topo-maps,' the reader can obtain a visual impression of the magnitude of the sound speed changes which occur across phase changes and as a function of pressure, density, or mass fraction. Consider two specific examples shown on the water-steam graph (Figure 1): the isentrope (*a*) at 7.4 J g^{-1} K^{-1} and the isentrope (*b*) at 3 J g^{-1} K^{-1}. The first of these (*a*) is located entirely within the vapor field at pressures above 1 bar. The spacings of the isobaric contours represent typical vapor sound speeds characteristic of steam, about 450 m s^{-1} at 1-bar pressure. At higher pressures the contours are more closely spaced (i.e., the topography is 'steeper'), indicating that the sound speed increases with increasing pressure. The second isentrope, (*b*), passes through two regions. It is in the liquid field above the saturation curve, and the high sound speed of liquid water (1500 m s^{-1}) is represented by the 'cliff' shown by the isobaric contours. The isentrope lies in the two-phase liquid-vapor field below the saturation curve; in this region, the typically low sound speeds of two-phase mixtures [*Kieffer*, 1977*b*] are represented as 'flatlands' by the isobaric contours. For example, in this region, at 1-bar pressure and for mass fractions less than 10^{-2}, the sound speed is a few tens of meters per second or less; it is 113 m s^{-1} at mass fraction 0.1. The sound speeds represented graphically in the two-phase region are 'equilibrium sound speeds' in the terminology used by *Kieffer* [1977*b*, p. 2901]. They are sound speeds under conditions where heat and mass transfer between the phases occur rapidly enough that thermodynamic equilibrium between the liquid and vapor phases is maintained; effects of surface tension on sound speed are not included in this representation.

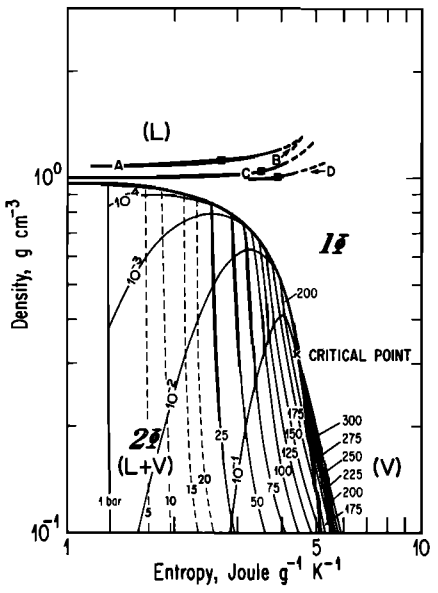

Fig. 3. Entropy-density relations for H_2O (enlargement of the top cycle of Figure 1) showing four typical continental geotherms: geotherm A, *MacGregor and Basu* [1974]; geotherm B, *Boyd and Nixon* [1973]; geotherm C, *Bird* [1975]; and geotherm D, *Mercier and Carter* [1974]. The base of the crust (40 km, 12 kbar) is indicated by a square on the geotherms A, C, and D. Dashed segments on the geotherms represent extrapolations above 800°C. Densities and entropies corresponding to the geotherms are calculated as described in the text.

Figures 1 and 2 show a light dashed vertical line which passes through the saturation curve at 1-bar pressure (labeled (*a*)): any geologic decompression which has an entropy less than the value at this line will result in conversion of the fluid at depth into a multiphase system before it reaches the surface pressure of 1 bar. In the case of H_2O the multiphase system is (liquid + vapor) (the ice stability fields are not considered here); in the case of CO_2 the multiphase systems encountered first by isentropes of decreasing entropy are: (solid + vapor), (liquid + vapor), (solid + liquid + vapor), and (solid + vapor).

4. Application to Geologic Problems

To illustrate the utility of these graphs, we examine here two processes assumed to occur isentropically: (1) ascent of magmatic fluids (e.g., in eruptions of volcanoes or diatremes) and (2) shock decompression of H_2O from pressures to 250 kbar.

Ascent of magmatic fluids. We have taken H_2O and CO_2 as representative end member compositions for magmatic fluids (H_2O for normal volcanic eruptions and, perhaps, some kimberlite eruptions; CO_2 for kimberlite and carbonatite eruptions). The effects of dissolved gases and salts are not included at this time for lack of thermodynamic data.

In order to specify the initial state of H_2O in the crust and mantle, we must specify entropies and densities of H_2O along representative continental geotherms. (Each geotherm was calculated to 1200°C. The maximum entropy obtained was 5.2 J g^{-1} K^{-1}.) Entropies and densities to 800°C (varying pressures, depending on the geotherm used) were obtained from the internally consistent data of *Keenan et al.* [1969], *Helgeson and Kirkham* [1974], and *Delany and Helgeson* [1978]. Entropies and densities at temperatures between 800° and 1200°C and at pressures greater than 10 kbar were extrapolated as follows: (1) densities, by a linear extrapolation of volume-temperature-pressure data [*Delany and Helgeson,* 1978, Figure 6]; (2) entropies, by a quadratic least-squares fit of entropy-temperature-pressure data [*Delany and Helgeson,* 1978, Figures 4 and 5] from 400°–800°C.

The entropy-density curves thus obtained for H_2O along representative continental geotherms are shown in Figure 3, which is an enlargement of the top cycle of Figure 1. Consider (using Figures 3 and 1) the isentropic ascent of H_2O originating at various depths along these geotherms.

H_2O originating at crustal depths (to the left of the square symbol on each geotherm) has, according to all geotherms, an entropy less than the critical point entropy of 4.4 J g^{-1} K^{-1}. Thus upon isentropic ascent, any H_2O, which is initially a supercritical fluid (SCF), ascends through the supercritical field into the liquid (*L*) field and then into the two-phase field (*L* + *V*), at which point part of the liquid vaporizes. From the isopleths plotted, it is possible to read the mass fraction of H_2O transformed into vapor by the time that the H_2O reaches the surface pressure of 1 bar, simply by reading the mass fraction at the point where the ascent path crosses the 1-bar isobar. For example, 20–30% of water ascending from the base of the crust (or upper mantle according to one geotherm) with an entropy of 3 J g^{-1} K^{-1} is transformed to vapor. A similar succession of phase changes (SCF → *L* → *L* + *V*) occurs if H_2O originates in the upper mantle at any depth which gives an initial entropy less than the critical point entropy of 4.4 J g^{-1} K^{-1}.

A different succession of phase changes is observed if H_2O originates with an entropy higher than the critical point entropy, e.g., deeper than 100 km on the *Mercier and Carter* [1974] geotherm; 60 km on the *Bird* [1975] geotherm, or 150 km on the *McGregor and Basu* [1974] geotherm. The H_2O is

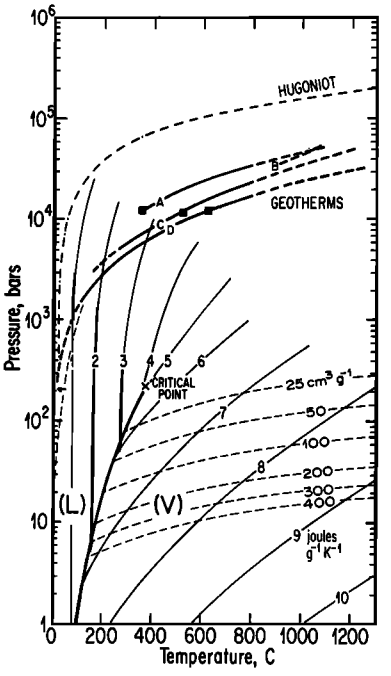

Fig. 4. Pressure-temperature relations for H_2O. Liquid and vapor fields, labeled (*L*) and (*V*), are separated by the saturation curve (heavy line). Contours of constant entropy (isentropes) are shown as solid lines, labeled in J g^{-1} K^{-1}. Contours of constant volume (isochores) are shown as dashed lines labeled in cm^3 g^{-1}. Contours of constant mass fraction (isopleths) in the two-phase region (shown on Figures 1 and 3) cannot be shown in pressure-temperature space because the two-phase region is degenerate along the saturation curve. The four geotherms A, B, C, and D are the same as in Figure 3, and the dashed segments are the same extrapolated regions. The Hugoniot [from *Rice and Walsh,* 1957] is the same as shown in Figure 7.

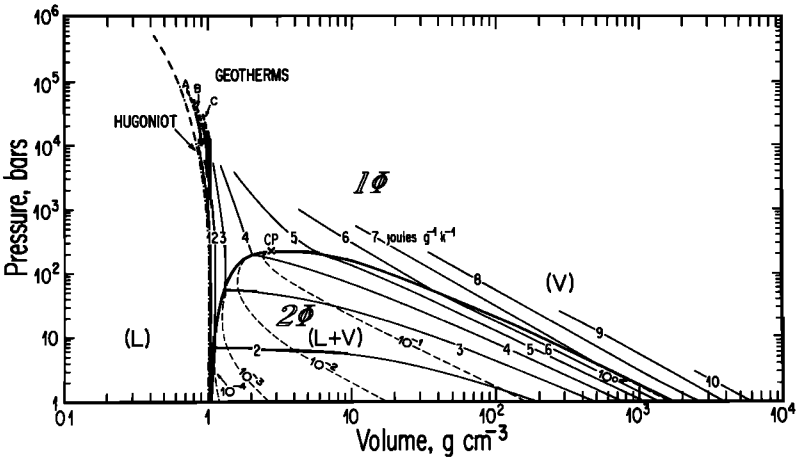

Fig. 5. Pressure-volume relations for H_2O. The single-phase field is shown as 1ϕ with the liquid (L) and vapor (V) regions labeled separately; the two-phase (liquid + vapor) field is shown as 2ϕ. Contours of constant entropy (isentropes) are shown as solid lines, labeled in J g^{-1} K^{-1}. Contours of constant mass fraction (isopleths) are shown as dashed lines. The three geotherms A, B, and C are the same as in Figure 3, and dashed segments are the same extrapolated regions. Geotherm D, not shown, overlaps A. The Hugoniot [from *Rice and Walsh*, 1957] is the same as shown in Figure 7.

originally in the supercritical state, but as it decompresses it passes into the vapor phase (see e.g., the isentrope descending at 5.0 J g^{-1} K^{-1}). If the entropy is less than 7.4 J g^{-1} K^{-1}, as it is for the limited temperature range calculated, then the fluid passes from the vapor phase into the two-phase field before it reaches the surface, i.e., liquid water is obtained by condensation of the vapor phase upon ascent. Examination of the mass fraction isopleths obtained on expansion to 1 bar from these geotherms indicates that at least 30%, and as much as 50% (at the critical point entropy), of the vapor fraction may condense on ascent of mantle fluids. This phenomenon is contrary to our intuition about the behavior of such systems.

Changes in acoustic properties of the fluids across the phase changes are dramatically shown on Figures 1 and 3 by variations in isobar spacings. For example, the supercritical fluid ascending with entropy of 3 J g^{-1} K^{-1} has the sound speed of a 'liquid' (approximately 1500 m s^{-1}), relatively independent of pressure until the two-phase field is entered at about 55 bars, as shown by the close spacing of the isobars in the liquid field. There is a dramatic discontinuous decrease in the sound speed, as shown by the change in spacing of the isobars (to about 30 m s^{-1}) upon entry into the two-phase field, and a further continuous decrease to a few meters per second as the fluid decompresses to 1-bar pressure. In contrast, although a supercritical fluid ascending with entropy of 5 J g^{-1} K^{-1} has the sound speed of a liquid at high pressures, the sound speed gradually decreases as the pressure decreases toward the saturation curve. As the fluid enters the two-phase field at about 190-bar pressure, there is a slight (about 10%) discontinuity in the sound speed. With further decompression to 1-bar pressure and condensation of a liquid from the vapor phase, the sound speed of the two-phase mixture continuously decreases to a final value of about 30 m s^{-1}. A detailed discussion of sound speeds in the water-steam system is given by *Kieffer* [1977*b*].

Although some of the same conclusions can be obtained by examination of graphs of other pairs of thermodynamic variables, we believe that the entropy-density graphs are unique in their ability to convey information of interest to both petrologists and geophysicists because information about the sound speed, the first derivative of a thermodynamic quantity, is so easily conveyed. To allow the reader to cross check the conclusions we have obtained for H_2O against those reached by use of more familiar thermodynamic graphs, we show the same adiabats and geotherms discussed above on a variety of graphs in Figure 4 (P-T), Figure 5 (P-V), and Figure 6 (T-S and P-S). As far as possible, the same thermodynamic information and schematic paths shown in Figures 1 and 3 are indicated on Figures 4, 5, and 6. Details are discussed in the figure captions.

As a specific example of this type of analysis, we consider the ascent of H_2O from a kimberlite reservoir. *McGetchin and Ullrich* [1973, p. 1844] calculated that H_2O originating in a kimberlite reservoir at 100-km depth, 1000°C would ascend nearly isothermally to 10-km depth (calculated temperature 954°C). At this pressure and temperature, H_2O has an entropy of about 5 J g^{-1} K^{-1} and therefore, upon further ascent, passes from supercritical fluid to vapor to (vapor + liquid) as discussed above. If nucleation of liquid droplets occurs rapidly so that the system maintains continuous local thermodynamic equilibrium, there will be a discontinuous change in the sound speed as the two-phase region is entered. (McGetchin and Ullrich assume supercooling of the vapor and thus do not deal with the possible two-phase flow problem.) It is well known that sound speed discontinuities give rise to perturbations in the fluid flow [*Zeldovich and Razier*, 1966, chapter 1, sections 17, 18, 19, chapter 11, section 20]. Although calculations of details of the fluid flow properties are not within the scope of this paper, it seems reasonable that the fluid flow changes might be of sufficient magnitude to significantly affect the nature of the kimberlite eruption and the structure of the maar complex formed during kimberlite eruption because as much as 30–50% of the vapor can condense before 1-bar pressure is reached. In particular, since H_2O at 5 J g^{-1} K^{-1} enters the two-phase field at a pressure of about 200 bars, structures at or above depths where this pressure is reached ($\lesssim$1 km) might show features related to the transition to two-phase fluid flow.

Because of the lack of thermodynamic data for CO_2 at pressures above 3 kbar and temperatures above 150°C, it is not possible to estimate the properties of CO_2 along geotherms with sufficient accuracy to warrant the type of analysis done for H_2O along geotherms. Instead, we consider only a simple comparison of the behavior of CO_2 and H_2O originating under similar conditions in a kimberlite reservoir. In order to compare the behavior of CO_2 with H_2O, we extrapolate the entropy

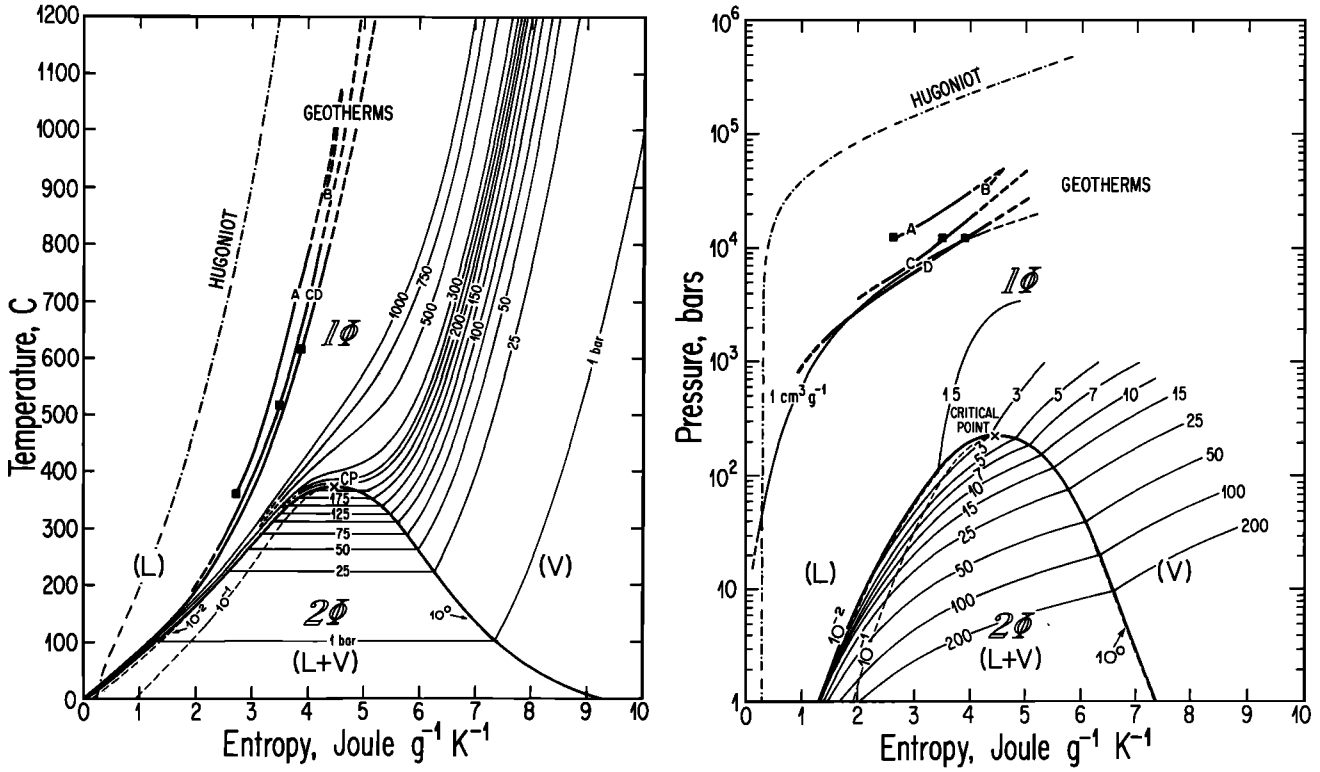

Fig. 6. (*a*) Temperature-entropy diagram and (*b*) pressure-entropy diagram for H_2O. The single-phase field is shown as 1ϕ with liquid (L) and vapor (V) regions labeled separately; the two-phase (liquid + vapor) field is shown as 2ϕ. Contours of constant pressure (isobars) are shown in Figure 6*a* as solid lines and of constant mass fraction (isopleths) in Figures 6*a* and 6*b* as dashed lines. Isochores, labeled in $cm^3\ g^{-1}$, are shown as solid lines in Figure 6*b*. The four geotherms A, B, C, and D are the same as those shown in Figure 3, and the dashed segments are the same extrapolated regions. The Hugoniot [from *Rice and Walsh*, 1957] is the same as shown in Figure 7.

of CO_2, known at 3 kbar, 150°C [*Newitt et al.*, 1956], to 1000°C through the thermodynamic identity

$$T\,dS = dH - V\,dP \tag{15}$$

which, at constant pressure, gives

$$dS = \frac{dH}{T} = \frac{C_P}{T}\,dT \tag{16a}$$

or

$$\int_{T_i}^{T_f} dS = \int_{T_i}^{T_f} \frac{C_P}{T}\,dT \tag{16b}$$

Taking T_i = 150°C (423 K), T_f = 1000°C (1273 K), C_P = const $\cong$ 1.5 J g^{-1} K^{-1} [*Newitt et al.*, 1956, p. 113], we obtain S(1000°C, 3 kbar) $\cong$ 5 J g^{-1} K^{-1}. This entropy is, coincidentally, the same as that of H_2O under similar conditions. Examination of Figure 2 shows that CO_2 with this entropy (in fact, with any entropy greater than 4.7 J g^{-1} K^{-1}, will ascend isentropically to the surface entirely as a vapor phase. Unlike H_2O, CO_2 ascending from 10 km, 1000°C will undergo no phase changes during ascent and therefore should not be subjected to discontinuities in the sound speed. This conclusion holds for systems with higher initial entropies or for systems in which the entropy increases upon ascent (up to entropies of 7.4 J g^{-1} K^{-1} for which H_2O will also remain in the vapor phase entirely to the surface). H_2O and CO_2 systems therefore should not be treated as qualitatively similar systems. Field evidence should be sought at kimberlite and carbonatite locales, particularly those exposed by erosion to depths of 1 km, to reflect possible structural variations arising from differing emplacement dynamics in H_2O-dominated versus CO_2-dominated systems.

Isentropic decompression of CO_2 with lower entropies than 4.7 J g^{-1} K^{-1} (e.g., originating at 1000°C, but at higher pressures than considered above) will result in phase changes before 1-bar pressure is reached as shown in Table 1. A rough estimate of the magnitude of the ($-V\,dP$) term in (15) suggests that the decrease in entropy due to pressure increases will be about 0.2 J g^{-1} K^{-1} $kbar^{-1}$. Therefore for temperatures greater than 1000°C (higher temperatures increase entropy) and pressures between 3 and 12 kbar (40 km), the entropy of CO_2 should be greater than 3 J g^{-1} K^{-1}. Hence for CO_2 fluids arising from crustal pressures, only cases 1, 2, 3, and 4 in Table 1 present plausible thermodynamic paths, although P-T conditions might be contrived to allow cases 5 and 6. Only additional high-pressure, high-temperature thermodynamic data for CO_2 will allow specific conclusions to be drawn, but plotting of such data on these entropy-density graphs will allow quick determination of possible phase changes during isentropic decompression of CO_2 from crustal and mantle pressures.

Isentropic release from shock compression. The history of H_2O undergoing shock decompression can be examined in detail with the use of entropy-density graphs if release 'adiabats' are assumed to be isentropes following vertical paths on the graph and if continuous equilibrium is assumed. The Hugoniot of water from 40 to 450 kbar is shown on Figure 7. The Hugoniot is centered at 1 bar, 20°C.

TABLE 1. Isentropic Decompression Paths for CO_2 From Crustal or Mantle Pressures to 1 Bar

Entropy Range S, J g^{-1} K^{-1}	Phase Changes
1. >4.7	SCF → V
2. 4.7–4.2 (TP1)	SCF → V → (S + V)
3. 4.2–3.55 (CP)	SCF → V → (V only at TP1) → (S + V) or SCF → V → (L + V) → (S + V)
4. 3.55–2.64 (TP2)	SCF → L → (L + V) → (S + V) or SCF → L → (L only at TP2) → (S + V)
5. 2.64–1.72 (TP3)	SCF → L → (L + S) → (S + V) or SCF → L → (S only at TP3) → (S + V)
6. <1.72	{SCF → L → S}* → (S + V)

SCF, supercritical fluid; S, solid; V, vapor; L, liquid. TP1 refers to the entropy of vapor at the triple point; TP2, the entropy of liquid at the triple point; TP3, the entropy of solid at the triple point; and CP, the entropy of the critical point.

*Unknown because melting curve data do not exist.

Hugoniot states less than 50 kbar have entropies less than that required for vaporization of H_2O on release to 1-bar pressure. A vertical release isentrope from such a shock state lies entirely within the liquid water field at all pressures above 1 bar, as can be seen by examination of the point where the 1-bar isobar intersects the saturation curve on Figures 1 or 7.

Hugoniot states above 50 kbar have entropies sufficient to allow partial vaporization of H_2O on release to 1-bar pressure. The isobars and isopleths plotted on the entropy-density graphs allow determination of the approximate pressure at which vaporization begins and of the mass fraction vaporized as a function of pressure on each release isentrope. For example, upon release from 60 kbar, vaporization begins at approximately 2-bars pressure, and ~6% of the liquid is vaporized by decompression to 1 bar. Similar behavior occurs to 275 kbar, from which decompression is through the critical point (220.9 bars, 4.4 J g^{-1} K^{-1}) and 50% of the liquid is vaporized upon decompression.

Upon decompression from pressures greater than 275 kbar, a different behavior is encountered. The compressed liquid expands isentropically around the critical point into the vapor phase, and as decompression brings the material to pressures lower than the critical pressure, a part of the vapor condenses to give a liquid fraction. For example, from 300 kbar, liquid begins condensing at about 225 bars, and nearly 50% of the vapor condenses. From 500 kbar, liquid begins condensing at 75 bars and approximately 20% of the vapor condenses. At very high shock pressures (order of a megabar), the unloading isentrope may remain entirely in the vapor region at all pressures greater than 1 bar (entropies greater than 7.4 J g^{-1} K^{-1}).

The behavior described above is thermodynamically required if isentropic conditions are obeyed. The kinetics of nucleation and growth of vapor bubbles (below 275 kbar) and liquid droplets (above 275 kbar) may control the actual conditions obtained. *Zeldovich and Razier* [1966, p. 764], in an analysis of the vaporization of solids by shock waves, suggest that the rate of nucleation of vapor bubbles or liquid droplets is so slow that the isentropes observed would actually be those of superheated liquids or subcooled vapors. However, there is ample evidence from laboratory equation-of-state measurements and petrographic properties of shocked rocks initially containing water that at least partial vaporization occurs (summarized by *Kieffer et al.* [1976, pp. 73–83]); the degree to which equilibrium is obtained has not been determined. Experimental evidence for condensation on release from high shock pressures does not appear to exist but should be obtainable in laboratory experiments with technology currently available, and the experiments would contribute a great deal to our understanding of isentropic processes and phase change kinetics under shock conditions since sufficient thermodynamic data exist to specify what the equilibrium states should be.

5. CONCLUSIONS

According to the two inequalities presented in (10*a*) and (10*b*), the flow of single-phase magmatic fluids and the rarefaction expansion of low viscosity liquids and gases may be considered to be approximately isentropic. Entropy-density graphs provide a useful way of envisioning changes in thermodynamic parameters for isentropic processes. Consideration of isentropic ascent of H_2O originating along various geotherms suggests that H_2O originating in the crust (S < 4.4 J g^{-1} K^{-1}) isentropically decompresses from a supercritical fluid to a liquid to a partially vaporized state, whereas H_2O originating in the upper mantle isentropically decompresses from a supercritical fluid to a vapor to a partially condensed state, with at least 30% and as much as 50% of the vapor condensing. A similar progression of phase changes is predicted for H_2O released from shock Hugoniot states: vaporization on release from shock states lower than 275 kbar, condensation upon release from higher pressures. Decompression entirely within the vapor field is the most likely behavior of CO_2 originating in kimberlite locales (assuming origin at 100 km, 1000°C, and isothermal ascent to 10 km, 1000°C, S = 5 J g^{-1} K^{-1}). A complex series of phase changes may occur upon isentropic decompression of CO_2 from entropies below 4.7 J g^{-1} K^{-1}. H_2O and CO_2 originating under similar conditions in kimberlite systems will not show qualitatively similar thermodynamic or fluid dynamic behavior because H_2O may partially condense during ascent, whereas CO_2 will remain in the vapor-alone field.

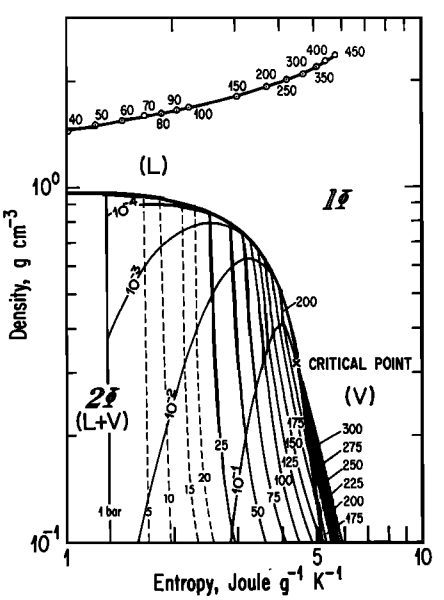

Fig. 7. Entropy-density relations for H_2O (enlargement of the top cycle of Figure 1) showing the shock Hugoniot of *Rice and Walsh* [1957]. Pressures are labeled in kilobars. The dashed line passes through the critical point. The Rice and Walsh Hugoniot data in Figures 4, 5, 6, and 7 (P, T, ρ, S, and V) are not internally consistent with the *Delany and Helgeson* [1978] data, which were only indirectly based on the Rice and Walsh data through *Jüza*'s [1966] equation-of-state.

Acknowledgments. This work was accomplished while S.W.K. was an Alfred P. Sloan Research Fellow, and she gratefully acknowledges the support of the Alfred P. Sloan Foundation. The work was also supported by NASA grant NSG 7052 and NSF grant 77-00789. We thank A. Boettcher, F. Busse, G. Schubert, and G. Ernst of UCLA for helpful comments.

REFERENCES

Ahrens, T. J., and J. T. Rosenberg, Shock metamorphism: Experiments on quartz and plagioclase, in *Shock Metamorphism of Natural Materials,* edited by B. French and N. Short, Mono, Baltimore, Md., 1968.

Batchelor, G. K., *An Introduction to Fluid Dynamics,* 615 pp., Cambridge University Press, London, 1967.

Bird, P., Thermal and mechanical evolution of continental convergence zones: Zagros and Himalayas, Ph. D. thesis, 423 pp., Mass. Inst. of Technol., Cambridge, 1975.

Boyd, F. R., and P. H. Nixon, Structure of the upper mantle beneath Lesotho, *Carnegie Inst. Washington Yearb., 72,* 431–449, 1973.

Bradley, J. N., *Shock Waves in Chemistry and Physics,* Methuen, London, 1962.

Bridgman, P. W., Change of phase under pressure, I, The phase diagram of eleven substances with especial reference to the melting curve, *Phys. Rev., 3,* 153–203, 1914.

Delany, J. M., and H. C. Helgeson, Calculation of the thermodynamic consequences of dehydration in subducting oceanic crust to 100 KB and >800°C, *Amer. J. Sci., 278,* 636–686, 1978.

Helgeson, H. C., and D. H. Kirkham, Theoretical prediction of the thermodynamic behavior of aqueous electrolytes at high pressures and temperatures, I, Summary of the thermodynamic/electrostatic properties of the solvent, *Amer. J. Sci., 274,* 1089–1198, 1974.

Jüza, J., An equation of state for water and steam, Steam tables in the critical region and in the range from 1,000 to 100,000 bars, *Rozpr. Cesk. Akad. Ved. Rada Tech. Ved., 76,* 3–121, 1966.

Keenan, J. H., F. G. Keyes, P. G. Hill, and J. G. Moore, *Steam Tables,* 196 pp., John Wiley, New York, 1969.

Kieffer, S. W., Geysers: A hydrodynamic model for the early stages of eruption, *Geol. Soc. Amer. Abstr. Programs, 7,* 1146, 1975.

Kieffer, S. W., Fluid dynamics during eruption of water-steam and magma-gas systems: Geysers, maars and diatremes (extended abstract), in *Second International Kimberlite Conference,* American Geophysical Union, Washington, D. C., 1977*a*.

Kieffer, S. W., Sound speed in liquid-gas mixtures: Water-air and water-steam, *J. Geophys. Res., 82,* 2895–2904, 1977*b*.

Kieffer, S. W., P. P. Phakey, and J. M. Christie, Shock processes in porous quartzite: Transmission electron microscope observations and theory, *Contrib. Mineral. Petrol., 59,* 41–93, 1976.

MacGregor, I. D., and A. R. Basu, Thermal structure of the lithosphere: A petrologic model, *Science, 185,* 1007–1011, 1974.

McGetchin, T. R., and G. W. Ullrich, Xenoliths in maars and diatremes with inferences for the moon, Mars, and Venus, *J. Geophys. Res., 78,* 1833–1853, 1973.

McQueen, R. G., and S. P. Marsh, Equation of state for nineteen metallic elements from shock-wave measurements to two megabars, *J. Appl. Phys., 31,* 1253–1269, 1960.

Mercier, J. C., and N. L. Carter, Pyroxene geotherms, *J. Geophys. Res., 80,* 3349–3362, 1974.

Newitt, D. M., M. U. Pai, N. R. Kuloor, and J. A. W. Huggill, Carbon dioxide, in *Thermodynamic Functions of Gases,* vol. 1, edited by F. Din, Butterworths, London, 1956.

Rice, M. H., and J. M. Walsh, Equation of state of water to 250 kilobars, *J. Chem. Phys., 26,* 825–830, 1957.

Rumble, D., The adiabatic gradient and adiabatic compressibility, Annual Report of the Director of the Geophysical Lab, *Carnegie Inst. Washington Yearb., 75,* 651–655, 1976.

Sanford, M. T., E. Jones, and T. McGetchin, Hydrodynamics of caldera-forming eruptions, *Geol. Soc. Amer. Abstr. Programs, 7,* 1257, 1975.

Shaw, H. R., Comments on viscosity, crystal settling and convection in granitic magmas, *Amer. J. Sci., 263,* 120–152, 1965.

Thompson, P. A., *Compressible-Fluid Dynamics,* 665 pp., McGraw-Hill, New York, 1972.

Zeldovich, Ya. B., and Yu. P. Razier, *Physics of Shock Waves and High-Temperature Hydrodynamic Phenomena,* vols. 1 and 2, Academic, New York, 1966.

(Received March 27, 1978;
accepted October 6, 1978.)